

## Supporting Information

### Highly Reversible Switching from P- to N-type NO<sub>2</sub> Sensing in Monolayer Fe<sub>2</sub>O<sub>3</sub> Inverse Opal and Associated P-N Transition Phase Diagram

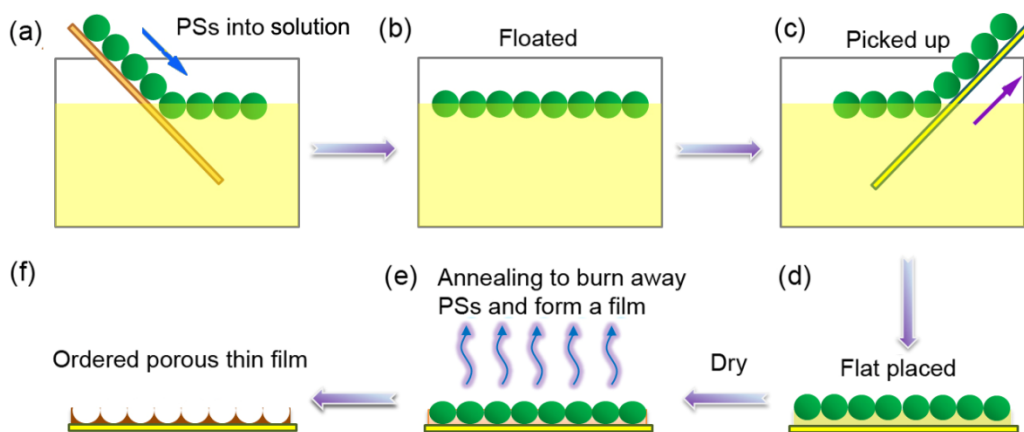
Zhengfei Dai,<sup>a</sup> Chul-Soon Lee,<sup>a</sup> Yahui Tian,<sup>a</sup> Il-Doo Kim,<sup>b</sup> and Jong-Heun Lee<sup>a,\*</sup>

<sup>a</sup>Department of Materials Science and Engineering, Korea University, Seoul 136-713, Republic of Korea;

<sup>b</sup>Department of Materials Science and Engineering, Korea Advanced Institute of Science and Technology, Daejeon, 305-701, Republic of Korea

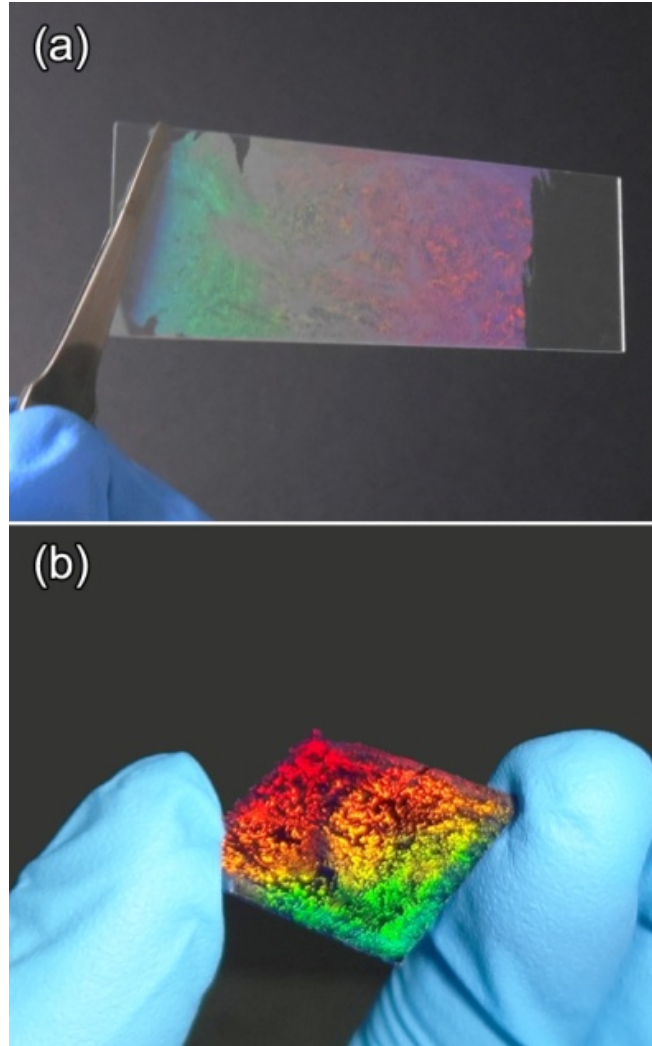
\* To whom correspondence should be addressed. E-mail: [jongheun@korea.ac.kr](mailto:jongheun@korea.ac.kr)

Figure S1. Zhengfei Dai *et al.*



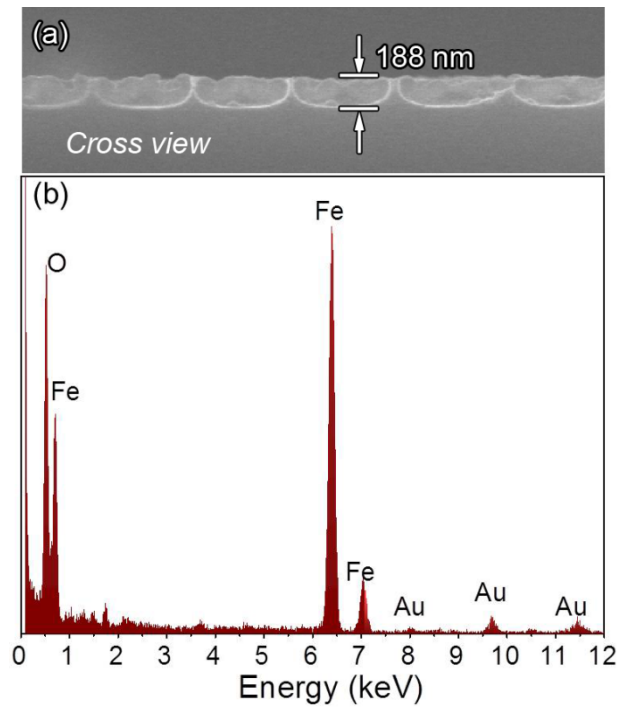
**Figure S1.** Schematic illustration of the fabrication strategy for honeycomb-like Fe<sub>2</sub>O<sub>3</sub> ordered porous thin films. (a) A flat glass slide covered with a colloidal monolayer of PS spheres is slowly dipped into a mixed precursor solution containing Fe<sup>3+</sup>. (b) The colloidal monolayer floats on the surface of the solution. (c) The floating monolayer is extracted and directly attached to the sensing substrate. (d) The substrate covered with the monolayer is laid out flat and dried. (e) The dried sample is annealed at high-temperature to remove the PS spheres, leading to (f) the final honeycomb-like ordered macroporous thin film.

**Figure S2.** Zhengfei Dai *et al.*



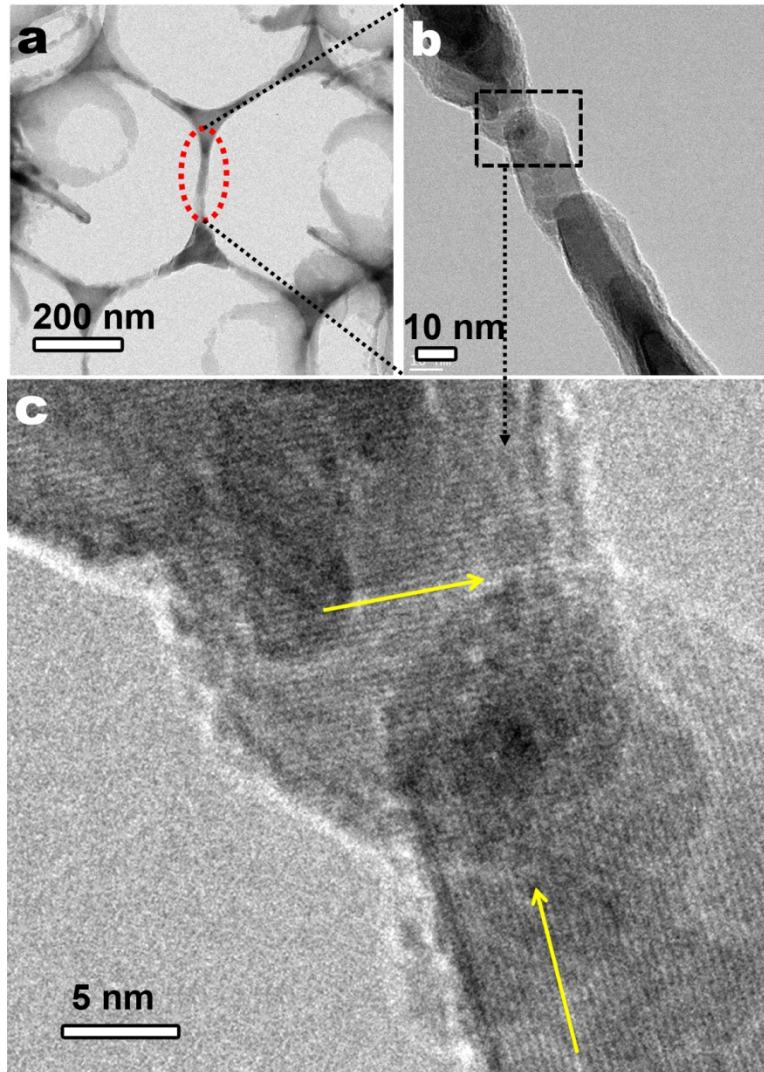
**Figure S2.** Photographs of (a) a self-assembled monolayer of PS spheres (500 nm in diameter) on a glass slide and (b) a template-directed ordered porous  $\text{Fe}_2\text{O}_3$  thin film on a silicon substrate.

**Figure S3.** Zhengfei Dai *et al.*



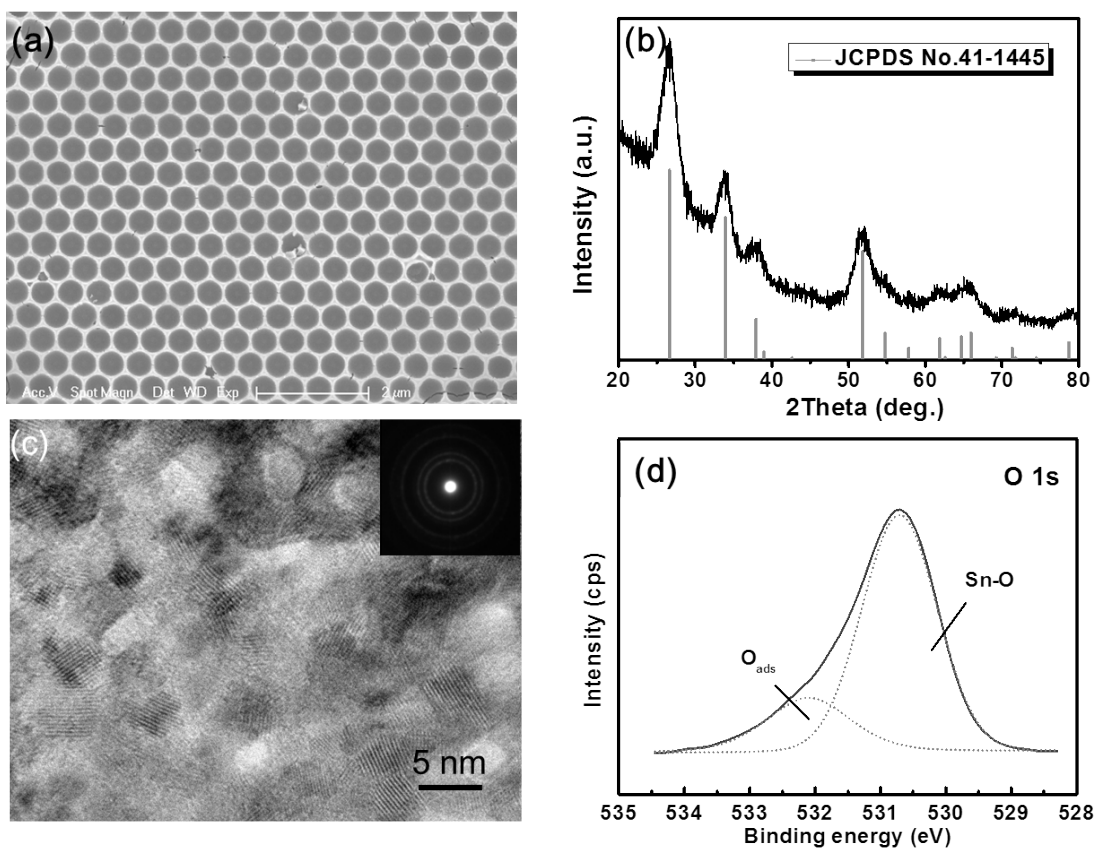
**Figure S3.** (a) Cross-sectional SEM image and (b) EDX pattern obtained from the ordered porous  $\text{Fe}_2\text{O}_3$  thin films.

Figure S4. Zhengfei Dai *et al.*



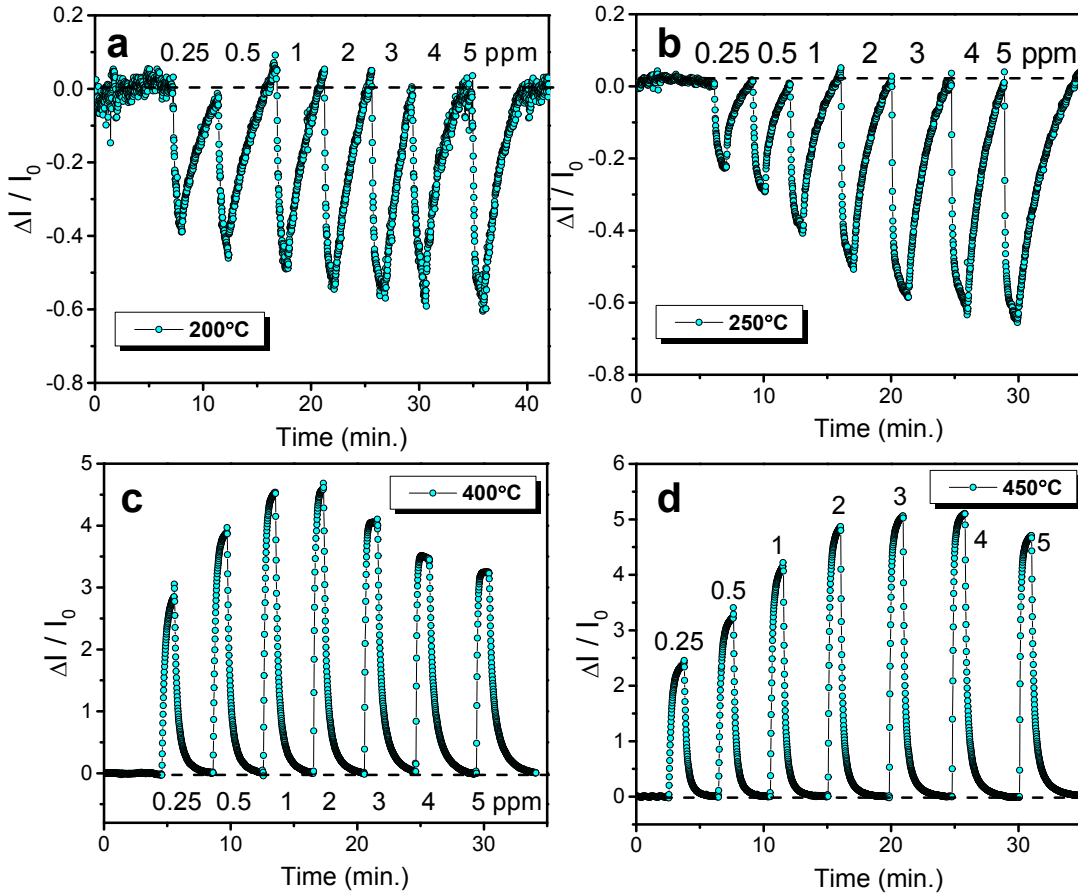
**Figure S4.** (a–c) TEM images at different levels of magnification of the channel between two adjoining 3-fold rotocenters in the  $\text{Fe}_2\text{O}_3$  pores. The yellow arrows in (c) indicate different crystal domains.

Figure S5. Zhengfei Dai *et al.*



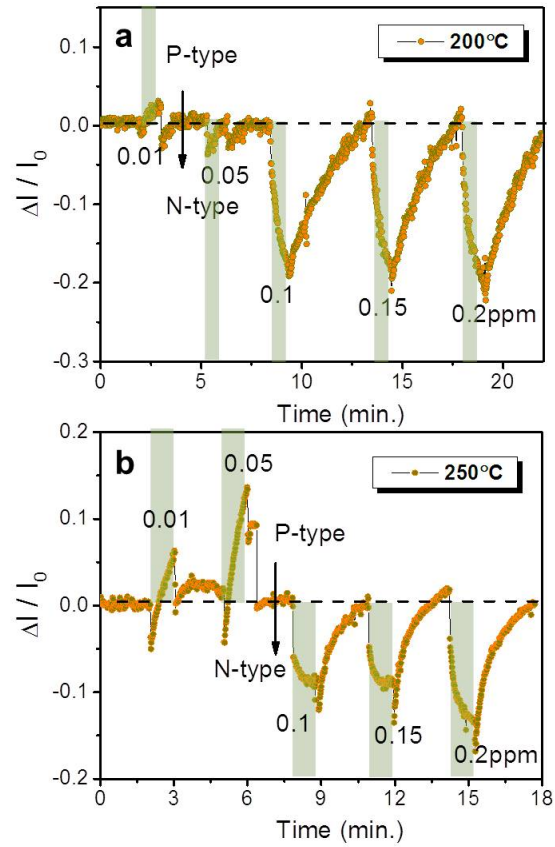
**Figure S5.** (a) SEM image, (b) XRD pattern, (c) TEM image and (inset) SAED pattern, and (d) O1s core level XPS spectrum of template-directed ordered porous SnO<sub>2</sub> thin films on a silicon substrate. The two peaks in (d), at 530.7 eV and 532.1 eV, are ascribed to Sn-O in SnO<sub>2</sub> and to surface adsorbed O groups, respectively.

Figure S6. Zhengfei Dai *et al.*



**Figure S6.** Sensing responses to 0.25–5 ppm  $\text{NO}_2$  of the porous  $\text{Fe}_2\text{O}_3$  sensor at (a) 200 °C, (b) 250 °C, (c) 400 °C and (d) 450 °C.

**Figure S7.** Zhengfei Dai *et al.*



**Figure S7.** Sensing responses to 10–200 ppb  $\text{NO}_2$  of the porous  $\text{Fe}_2\text{O}_3$  sensor at (a) 200 °C and (b) 250 °C.

Figure S8. Zhengfei Dai *et al.*

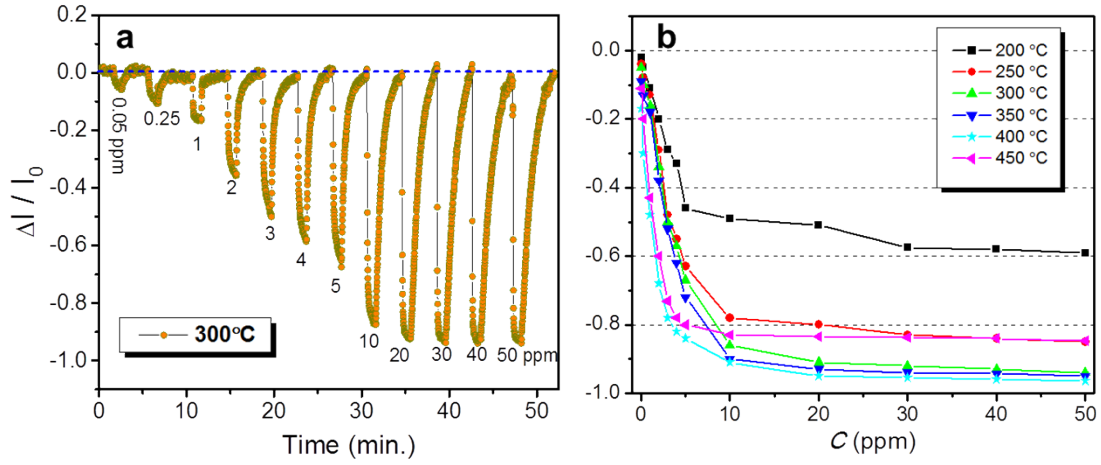


**Figure S8.** Sensing responses to 0.05–50 ppm NO<sub>2</sub> of a porous SnO<sub>2</sub> sensor at (a) 300 °C and (b) 200–450 °C.

Figure S9. Zhengfei Dai *et al.*

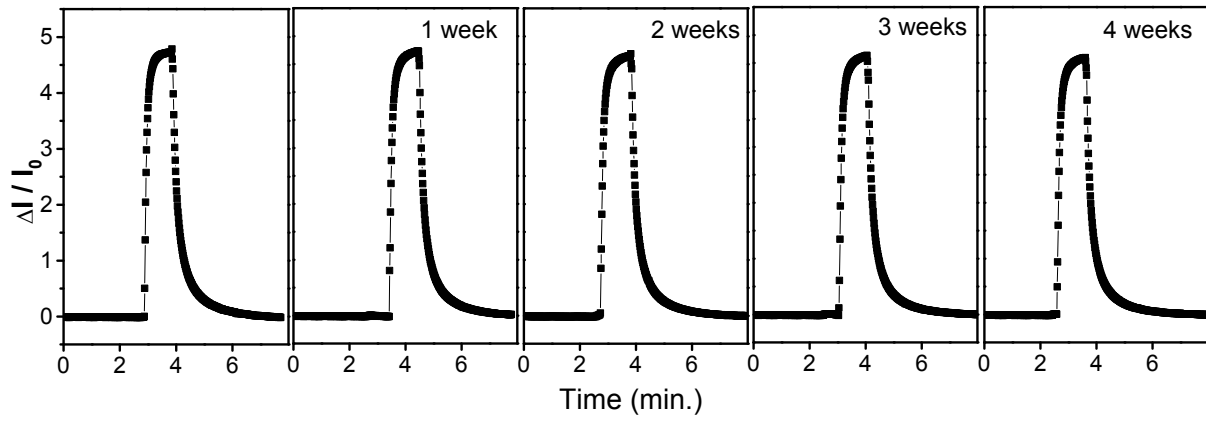
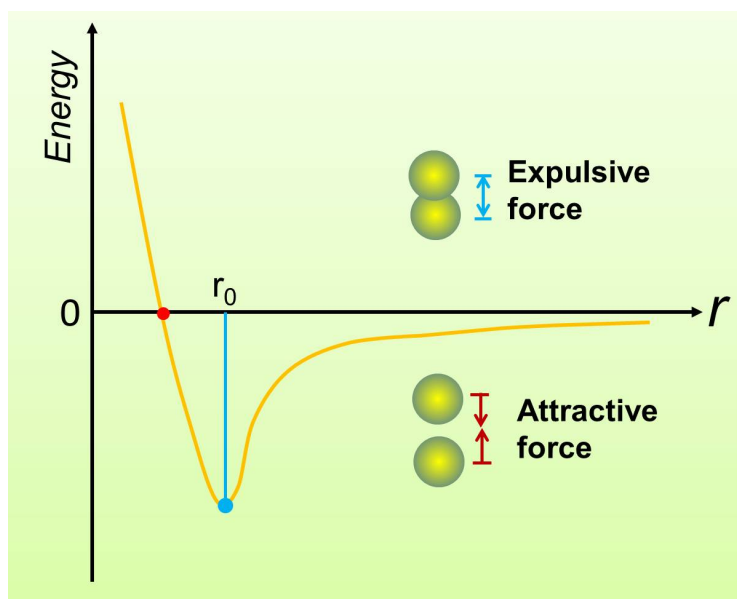


Figure S9. The stability of the sensing response of the  $\text{Fe}_2\text{O}_3$  device at  $450\text{ }^\circ\text{C}$  over 4 weeks.

**Figure S10.** Zhengfei Dai *et al.*



**Figure S10.** Schematic illustration of the well-known Lennard-Jones potential.